INTERNATIONAL ATOMIC ENERGY AGENCY
UNITED NATIONS EDUCATIONAL, SCIENTIFIC AND CULTURAL ORGANIZATION
INTERNATIONAL CENTRE FOR THEORETICAL PHYSICS
I.C.T.P., P.O. BOX 586, 34100 TRIESTE, ITALY. CABLE CENTRATOM TRIESTE

SMR.550 - 12

SPRING COLLEGE IN MATERIALS SCIENCE ON
"NUCLEATION, GROWTH AND SEGREGATION IN MATERIALS
SCIENCE AND ENGINEERING"
(6 May - 7 June 1991)

STABILITY OF MICROSCOPIC CLUSTERS

(PART III)

J.A. ALONSO
Departamento de Fisica Teorica y Fisica Atomica y Nuclear
Facultad de Ciencias
Universidad de Valladolid
Valladolid
Spain

STABILITY OF MICROSCOPIC CLUSTERS

3rd Lecture: Selected topics on metal clusters

J. A. ALONSO

Lectures to be delivered at:
Spring College in Materials Science on
"Nucleation, growth and segregation in Materials Science and Engineering"
(International Centre for Theoretical Physics, Triestre, May-June 1991)

1. SHELL EFFECTS IN NOBLE METAL CLUSTERS

Experiments for noble metal clusters (Cu_N, Ag_N, Au_N) indicate the existence of shell-effects, similar to those observed in alkaline clusters. Katakuse and coworkers[1,2] have recorded mass spectra for clusters produced as secondary ions after bombarding a sheet of the metal with accelerated inert gas ions. Figure 1 shows the mass distribution for Ag_N^+ up to a cluster size N = 100, plotted in a logarithmic scale, and fig. 2 is a raw spectrum for N = 50 to N = 250. The ion intensity decreases pseudo-exponentially with N. This tendency is generally seen in secondary ion mass spectra of clusters. Superimposed on this general decrease, two kinds of anomalies were observed. One anomaly is the odd-even alternation of the cluster intensity, in which the intensity of odd-N clusters is greater than that of even-N clusters. This odd-even effect will be discussed later on. The other anomaly was observed at peculiar values of N. At the sizes N = 3, 9, 21, 35, 41, 59, 93, 139 and 199 the cluster intensity decreases steeply. The silver atom in its ground state has a closed d-shell and a single s valence electron. If we use a model similar to that employed for alkaline clusters, we can assume the 5s valence electrons in a silver cluster interacting with a smooth effective potential of a spherical well. The experimental technique used by Katakuse is such that the Ag clusters are born ionized. So the recorded mass spectrum reflects the relative stabilities of ionized clusters Ag_N^+, in which the number of valence electrons is N-1. From the list given above we find N-1 = 2, 8, 20, 34, 40, 58, 92, 138 and 198. These are the shell-closing numbers already known for alkaline clusters. Mass spectra for Cu_N^+ and Au_N^+ also show these magic numbers[1,2] (see Fig. 3). Even more, negatively charged clusters (Cu_N^-, Ag_N^-, Au_N^-) can also be obtained by the same experimental technique. Figure 3 also shows the size distribution of Cu_N^- clusters for N < 70. The similarity with the spectrum of Cu_N^+ is evident . The shell-closing numbers of Cu_N^- cluster are observed for N = 7, 19, 33, 39, 57, ..., but notice that Cu_N^- contains N+1 valence electrons. As a summary Table 1 gives a complete list of the shell-closings observed in the mass spectra of positive and negative Cu, Ag and Au clusters.

Few measurements of the ionization potential (IP) of noble metal clusters have been performed to our knowledge. Those performed by Powers et al[3] give only lower and upper bounds to IP. Even so, the drop of IP between Cu_8 and Cu_9, corresponding to the opening of the 1d shell, is indicated by the experiments.

In contrast, many photoelectron spectroscopy studies on noble metal cluster anions (Cu_N^-, Ag_N^-, Au_N^-) have been performed. These photodetachment experiments give direct information on the electron affinity EA. This magnitude is defined

$$EA = E(M_N) - E(M_N^-) \qquad (1)$$

that is, the different between the energies of the neutral and the negatively ionized cluster. Figure 4 gives a schematic representation of the ionization and detachment processes.

In the photodetachment experiments a negative cluster, for instance Ag_N^-, is irradiated with laser light of fixed energy $h\nu$. The photon ionizes an electron from the highest occupied molecular orbital (HOMO) or from a deeper orbital (transitions (1) and (2) in Fig. 5 respectively). If the corresponding neutral cluster had closed shells then the photoelectron is ejected from the lowest unoccupied molecular orbital (LUMO). The difference $h\nu$-E_{kin}, where E_{kin} is the kinetic energy of the detached electron, gives a direct measure of the orbital position. The photoelectron spectra of a series of silver cluster anions, taken by

Gantefor et al[4], is shown in Figure 6. Photoelectron thresholds, as estimates of the adiabatic electron affinity, are marked by a horizontal solid bar. This energy corresponds to a transition from Ag_N^- into the neutral Ag_N ground state. Often the ground state geometries of Ag_N^- and Ag_N are not the same. Then the maximum indicated by the arrow in the figure gives the "vertical" detachment energy (vertical means that the cluster geometry does not change during the detachment process). At higher electron binding energies additional lines indicate transitions into electronically excited states of the neutral Ag_N .

The colorfulness of the photoelectron spectrum is well demonstrated in the figure. Every species has its own fingerprint. The electronic structure often does not change smoothly when the size is changed.

The measured detachment energies of Ag_N^- are plotted in Fig. 7. Basic features are the pronounced even/odd oscillation and the drops at N=7 and N=19. Since Ag_N^- contains N+1 valence electrons, those drops indicate major shell closings $(1s)^2$ $(1p)^6$ and $(1s)^2$ $(1p)^6$ $(1d)^{10}$ $(2s)^2$ respectively.

These features encourage one to apply the jellium model to the fine details of the photoelectron espectra. The electron affinities of Cu clusters obtained by Penzar and Ekardt[5] using the spheroidally deformed jellium model (see 2nd Lecture) are included in Fig. 8. Over a wide N-range the calculation qualitatively agrees with the meaurements. A general offset and an overestimation of the shell closing, however, remains. The second effect is an intrinsic feature of the jellium model.

2. d ELECTRONS IN NOBLE METAL CLUSTERS. EVOLUTION OF THE d BAND

Section 1 has provided us with evidence that the electronic structure of noble metal clusters near the top of the occupied cluster orbitals (i.e. near the "Fermi energy" of the cluster) appears to be well described by a simple shell model. The physical picture here is essentially the same as in the free electron theory of metals, but now with spheroidal boundary conditions at the surface of the cluster. While these results are impresive, it is still true that the electronic structure being probed is only that of the most weakly bound electrons. A reasonable next question is how much deeper down into the band structure of these metal clusters can we probe and understand. For example, in the case of copper, there is the question of how the atomic 3d orbitals combine in the clusters and how the band of cluster levels derived from these 3d orbitals evolves to form the 3d band of Bloch waves in the extended crystal.

Cheshnovsky et al have used Ultraviolet Electron Spectroscopy (UPS) to probe the 3d band of mass-selected negative copper clusters[6]. Fig. 9 shows the UPS spectra for clusters ranging from the single atom (top) to a cluster with 410 atoms (bottom). Probing the d-band requires high enough photon energies (compare with Fig. 6). The threshold for photoelectron ejection (indicated by the black dots in Fig. 9) gives an estimate of the electron affinity of Cu_N, but since this topic has already been discussed in Section 1 above, we concentrate now on the large peak, roughly 2 eV higher than the weak initial features, which moves smoothly with cluster size. For the small clusters its position merges smoothly with the position of the $^2D_{5/2}$ and $^2D_{3/2}$ levels of the copper atom. For the large clusters, allowing for a 0.6 eV shift to match the

work function, the large peak matches well with the sharp onset of the 3d band in the UPS of bulk copper[7]. For all these clusters therefore it seems safe to attribute this feature to the photodetachment of primarily 3d-type electrons, and to chose the rising edge of this feature to be a measure of the top of the "3d band". Taking half the peak height as the 3d onset we have marked these energies both in Figures 9 and 10.

Unlike the large size-dependent variations associated with the 4s electrons, the 3d features shift monotonically with the cluster size, consistent with the different valence nature of these spectral features. The 3d electrons are more core-like and should be only mildly influenced by the details of the cluster surface. An interesting observation is that the onset of the 3d band sharpens as N increases. This is interpreted by Cheshnovsky et al as an indication that the larger clusters may already de crystalline.

In the conventional solid state physics of noble metals the valence band contains the localized d electrons as well as the extended s electrons, and the s-d mixing is substantial[8]. The picture of valence electrons is far from that of the free electrons in simple metals. Then, it is intriguing how well the shell model works also in noble metal clusters.

To answer this question Fujima and Yamaguchi[9] have performed self-consistent calculations using a method known as the DV-Xα (Discrete Variational exchange-alpha) method[10]. The results of such a calculation for Cu_{13} and C_{12} clusters with icosahedral symmetry are given in Figure 11. Many electronic levels are degenerate in the region around -0.3 a.u. There are 17 and 16 levels for Cu_{13} and C_{12} respectively in this region. A charge population analysis shows that most of them are composed of more than 90% 3d orbitals (see Fig. 11 a). Among the 17

levels of Cu_{13}, the lowest one, ^1H_g, is isolated from the others. It has 72% 3d character of the central atom and it bonds weakly with the 3d levels of surrounding atoms. The remaining 16 levels correspond to the 16 levels of Cu_{12}. The energy width of the 16 level group is about 0.7 a.u., which is comparable to the d-band width of Cu metal bulk. The charge analysis also clarifies that the other levels are composed of mainly the 4s and 4p orbitals.

These facts imply that the 3d electrons of Cu clusters do not mix with the 4s and 4p electrons. The charge distributions of Fig. 12 are a clear demostration of this fact. The 3d charge is localized around atoms whereas the 4s, 4p charge is extended over the whole cluster.

The ^1A_g, $^1T_{1u}$, ^2H_g, etc are levels with s-p character. If we neglect the 3d electrons the sequence of electronic levels can be reproduced fairly well by considering an spherical model potential with appropriate parameters: in the case of Cu_{13} this is a harmonic oscillator potential with an small anharmonic term; in the case of Cu_{12}, one must add to this potential a 3-dimensional Gaussian potential barrier which simulates the lack of central atom in the cluster. The results are shown in parts (c) and (d) of Fig. 11. The one-to-one correspondence between the energy levels of the DV-Xα method and the simple model potential leads to the conclusion that the shell model is applicable to Cu clusters, since the s-p valence electrons are distributed nearly spherically and the localized d electrons do not mix with the extended sp electrons.

With Figure 11 in mind one still may wonder what would happen to a cluster Cu_N with $N < 8$ since the $^1T_{1u}$ level of Cu_{12} and Cu_{13} is below the d levels in this figure. The results of DVXα calculations for Cu_6 (octahedron), Cu_8 (cube), Cu_{13} (cuboctahedron), Cu_{15} (rhombic

dodecahedron), and Cu_{19} (combined cluster of cuboctahedron and octahedron) are shown in Figure 13. For Cu_6 the d levels are located between the 1s and 1p levels of the shell model. The level $^1T_{1u}$, corresponding to the level 1p, is the Fermi level. Two holes exist on this level above the nearly degenerate d levels, which are occupied. The energy levels of Cu_8 are critical, that is, the d levels are located just above the 1p level. The level $^1T_{1u}$, corresponding to 1p, has about 50% 3d character. The Fermi level E_u is filled by almost 100% 3d electrons. The d levels of Cu_{13} (Fig 13c) are located between the 1p and 1d levels of the shell model like in the icosahedral cluster of Fig. 11. In summary, Figure 13 shows that: (a) The Fermi energy is nearly constant (-0.17 a.u.). (b) The 3d orbitals have nearly constant energies from -0.17 to -0.36 a.u. (c) Finally the d levels are located between the 1s and 1p levels of the shell model for $3 \leq N \leq 8$, between the 1p and 1d levels for $9 \leq N \leq 18$, between the 1d and 2s levels for $19 \leq N \leq 20$, and so on. The d levels are filled.

3. GENERAL DISCUSSION OF THE IONIZATION POTENTIAL OF METALLIC CLUSTERS

The ionization potential IP is the energy necessary to extract one electron from the neutral cluster (see Fig. 4). For a macroscopic solid this is called the work function W. In this limiting case W can be expressed as the sum of three terms[11]

$$W = E_{es} + \mu_{xc} - E_F . \qquad (2)$$

where all contributions are taken here to be positive. The first, electrostatic term, E_{es} represents the surface barrier resulting from

the spilling of electron charge beyond the jellium boundary. The second, μ_{xc}, is the exchange and correlation contribution to the chemical potential of an uniform electron gas. These two terms mainly determine the depth of the potential well. The kinetic energy term, E_F, is the bulk Fermi energy. Lang and Kohn[11] calculate for bulk sodium, according to eq. (2), W = 0.91 + 5.28 - 3.13 = 3.06 eV, compared to an experimental value of 2.7 eV. For potassium, they give W = 2.74, compared to the experimental value 2.39 eV. Inclusion of ion pseudopotentials decreases the calculated values by ≈ 10%. We may conclude that the calculated work functions for the alkali metals are in reasonable agreement with experiment. Similar agreement was also obtained for several other simple metals.

When the size of the metallic piece is microscopic we must add a correction term. Eq(3) gives a widely used classical expression, obtained from simple electrostatic considerations on the energy to remove an electron from a uniformly conducting sphere[12,13]

$$IP = W + A\frac{e^2}{R} \qquad (3)$$

with A = 1/2. Here W is the bulk work function and R is the classical radius of the spherical cluster. The corresponding expression for the electron affinity is

$$EA = W - A'\frac{e^2}{R} \qquad (4)$$

with A'=1/2 also. Theoretical considerations based on density functional theory, which trascend the simple electrostatic arguments, indicate that eqs (3) and (4) should be improved substituting the constants $A = \frac{1}{2}$, $A' = \frac{1}{2}$ by $A = \frac{1}{2} - c$, $A' = \frac{1}{2} + c$. In this way we have

$$IP = W + \left(\frac{1}{2} - c\right)\frac{e^2}{R} \qquad (5)$$

$$EA = W - \left(\frac{1}{2} + c \right) \frac{e^2}{R} \qquad (6)$$

These equations are valid for large R, that is, when shell effects become negligible. The exact value of c is not known. Theoretical calculations within the framework of density functional theory give c in the range 0.07 - 0.08 (ref. 14), 0.07-0.12 (ref.15), or a little bit larger (c ≈ 0.14) (ref. 16). These values, in particular the last one, are consistent with the empirical value c ≈ 0.12 ±0.06 obtained from a recent photoemission study of very large Ag clusters containing 5000-40.000 atoms[17]. Numerous studies for medium size clusters, N≤100, of different metallic elements give a good fit to experiment with c = 1/8 = 0.125 (refs 18-20). Actually, Wood's image potential argument gives exactly c = 1/8 (ref. 21), which leads to

$$IP = W + \frac{3}{8} \frac{e^2}{R} \qquad (7)$$

$$EA = W - \frac{5}{8} \frac{e^2}{R} \qquad (8)$$

However, the image-potential argument has been criticized[12,22]. Further work, on the line of refs 14 - 16, should be welcome to further clarify the asymptotic behavior of IP and EA.

Figure 14 gives a comparison between the measured ionization potentials and equation (7). For the determination of R one assumes the relation $V_{cluster}=NV_{atom}$ between volumes, where $V_{cluster}$ is the volume of the cluster and V_{atom} is the volume per atom in the bulk solid. The magnitude actually plotted in Fig. 14 is IP-W versus 1/R, where W is the work function predicted on the basis of extrapolating the experimental data to 1/R = 0. Such extrapolations come very close to the accepted polycrystalline work functions for the simple metals. Significant differences between measured and extrapolated work

functions are, however, observed for some of the transition metals and in particular Hg. The straight line plotted corresponds to the slope 3/8 in eq. (7).

General agreement of spherical droplet predictions (slope and bulk extrapolation) with the ionization potential data has several implications: (1) The assumption of spherical symmetry is viable (N>10). (2) The size dependence of IP is overrindingly determined by changes in curvature above the level of quantum size effects, which are typically not larger than 10% of the IP. (3) Valence electrons are delocalized even for very small clusters.

Now Figure 15 compares the measured EAs of Al_N, In_N and Tl_N to eq.(8). A good agreement between measured and predicted values is again found. Around N=20, EA is still 2 eV below the corresponding polycrystalline work function, in agreement with the model. This result should not be interpreted as a proof of the good electrical conductivity of the cluster. Instead, the agreement might be an indication of the degree of electron delocalization. A small difference with respect to the IP plot of Fig. 14 is that the work function W used in Fig. 15 is the experimental one.

Finally, with respect to the comparison reported in Figures 14 and 15 one should keep in mind that the cluster radius has been estimated by assuming that atomic volumes have the same values as in the bulk solid. This is not strictly true. It is well known that a slight contraction of interatomic distances occurs in small clusters, although this effect is difficult to quantify[20,23].

4. ODD-EVEN EFFECTS IN CLUSTERS OF MONOVALENT METALLIC ELEMENTS

Superimposed to the smooth behavior describec by equations (7)

and (8) the experimental data on the ionization potentials and electron affinities shows two additional effects. One, which has already been discussed in other parts of these Lectures, is the shell-closing effect: IP drops abruptly when a new shell is opened up. The second effect, which can be observed in clusters of monovalent s-electron metals can be classified as an even-odd effect and is also apparent in the mass spectra. I give now some examples:

(i) In ionization potential measurements of alkalis (Na_N, N<20; K_N, N<20) even clusters systematically have slightly (0.1-0.2 eV) larger values than their N-odd neighbors (see Fig 2 of 2nd Lecture in this series).

(ii) An inverse effect is found for the electron affinity of noble metal clusters, with N-odd clusters having higher photodetachment thresholds[24] (see Figure 16).

(iii) The mass spectrum of both positive and negative ion clusters of noble metals obtained by ion bombardment shows an odd-even alternation in the abundances, with N-even clusters being less abundant than their N-odd neighbors (see Figs 1 and 2). This effect is observed up to N=20-40, the limit depending on the particular element and charge state (positive o negative charge).

iv) Sodium cluster photoionization efficiency (PIE) curves manifest an even-odd dependence on post-threshold ion yield (>0.5eV) above the vertical IP, which can be explained in terms of lower ionization-induced fragmentation rates for odd cluster ions. The effect is observable up to and including Na_{41}^+ (ref. 23). Fig. 17 shows PIE curves for Na_{14}-Na_{21} (see also Fig 3 in the 2nd Lecture in this series).

Several theoretical calculations have been able to reproduce the odd-even effects in the ionization potentials and binding energies. For instance, we mention the Hückel-Molecular Orbital Calculations of Lindsay et al[25] (see Figure 18 for the ionization potentials of Na_N and K_N), the density functional calculations of Martins et al[26] (see the Na panel in Fig. 18; these calculations use the local-spin-density approximation for the exchange and correlation effects, and substitute the ion cores by pseudopotentials), and the ab-initio CI (Configuration Interaction) calculations of Koutecky's group[27,28] (binding energies of clusters are given in Figure 19). However, even if the results in these figures clearly indicate that the theoretical calculations contain the ingredients needed to exhibit the odd-even effect, the microscopic origin of this effect has not been discussed, in our opinion, in enough detail.

There is a consensus that the odd-even effects can be explained in terms of stabilization due to electron pairing. In Figure 20 we show the evolution of the Hückel Molecular Orbital energies for the (calculated) most stable geometrical conformations of alkaline clusters with sizes N = 2 - 14. First of all there is a smooth decrease of the 1s orbital with increasing number of atoms. Also the manifold of 1p-type levels shows and overall decrease with increasing N. However, contrary to the predictions fo the spherical jellium model, the $1p_x$, $1p_y$ and $1p_z$ orbitals are not degenerate in energy. This splitting is a consequence of the fact that the cluster (and then the effective potential acting on the electrons) is not spherical. The magnitude of the energy separation between ($1p_x$, $1p_y$) and $1p_z$ orbitals reflects the degree of distortion from spherical symmetry. In clusters resembling an oblate ellipsoid (OE) the $1p_z$ orbital lies lower in energy than ($1p_x$, $1p_y$). For geometries best described as prolate ellipsoids (PE) the order of $1p_z$ and ($1p_x$, $1p_y$) is reversed. Doubly occupied p orbitals have a lower energy (are more stable) than singly occupied ones (see N=5, N=7). This is the spin-pairing effect. The splitting of p levels just described is a self-

consistent effect: when the external electronic shell is not fully occupied, the electron density is not spherically symmetric. This, in turn, induces a distortion of the cluster geometry away from the spherical shape which leads to the splitting of the p-levels. In summary, the splitting of the p-shell and the variation of the energy of the p-levels with cluster size explain the odd-even effects in stability and ionization potentials for N≤8. Similar arguments concerning the splitting of the d-shell, etc, rationalize the odd-even effect for larger clusters.

REFERENCES

1. I. Katakuse, T. Ichihara, Y. Fujita, T. Matsuo, T. Sakurai and H. Matsuda, Int. J. Mass Spectrom. Ion Proc. 67, 229 (1985); (b) 74, 33 (1986)
2. I. Katakuse, T. Ichihara, T. Matsuo, T. Sakurai and H. Matsuda, Int. J. Mass Spectrom. Ion Proc. 91, 99 (1989)
3. D.E. Powers, S.G. Hansen, M.E. Geusic, D.G. Michalopoulos and R.E. Smalley, J. Chem. Phys. 78, 2866 (1983)
4. G. Ganteför, M. Gausa, K.H. Meiwes-Broer and H.O. Lutz, J. Chem. Soc. Faraday Trans. 86, 2483 (1990)
5. Z. Penzar and W. Ekardt, Z. Phys. D 17, 69 (1990)
6. O. Cheshnovsky, K.J. Taylor, J. Conceicao and R.E. Smalley, Phys. Rev. Lett. 64, 1785 (1990)
7. W.F. Egelhoff and G.G. Tibbetts, Solid State Commun. 29, 53 (1979)
8. J.A. Alonso and N.H. March, Electrons in Metals and Alloys, Academic Press, London (1989)
9. N. Fujima and T. Yamaguchi, J. Phys. Soc. Japan 58, 1334 (1989)
10. J.C. Slater, The Calculation of Molecular Orbitals, John Wiley, New York (1979)
11. N.D. Lang and W. Kohn, Phys. Rev. B3, 1215 (1971)
12. G. Makov, A. Nitzan and L.E. Brus, J. Chem. Phys. 88, 5076 (1988)
13. W. A. de Heer and P. Milani, Phys. Rev. Lett, 65, 3356 (1990)
14. E. Engel and J.P. Perdew, Phys Rev. B 43, 1331 (1991)
15. M.E. Spina, M. Seidl and M. Brack, Proceedings of the Symposium on Atomic and Surface Physics 90, p. 426, Obertraum, Austria (1990)
16. A. Rubio, L.C. Balbás and J.A. Alonso, Physica B 167, 19 (1990)
17. U. Müller, A. Schmidt-Ott and H. Burstcher, Z. Phys. B 73, 103 (1988)
18. C. Bréchignac, Ph. Cahuzac, F. Carlier and J. Leygnier, Phys. Rev. Lett. 63, 1368 (1989)

19. M.M Kappes, M. Schär, P. Radi and E. Schumacher, J. Chem. Phys. 84, 1863 (1986)
20. K.H. Meiwes-Broer, in "Advances in metal and Semiconductor clusters", Vol 1: Spectroscopy and Dynamics, Ed. M. Ducan, J.A.I. Press (1991) (to be published)
21. D.M. Wood, Phys. Rev. Lett. 46, 749 (1981)
22. J.P. Perdew, Condensed Matter Theories, Vol. 4. Ed. J. Keller, Plenum Press, New York (1989), p. 149
23. M.M. Kappes, Chem. Reviews 88, 369 (1988)
24. J. Ho, K.M. Ervin and W.C. Lineberger, J. Chem. Phys. 93, 6987 (1990)
25. D.M. Lindsay, Y. Wang and T.F. George, J. Chem. Phys. 86, 3500 (1987)
26. J.L. Martins, J. Buttet and R. Car, Phys. Rev. B31, 1804 (1985)
27. V. Bonacic-Koutecky, I. Boustani, M. Guest and J. Koutecky J. Chem. Phys. 89, 4861 (1988)
28. V. Bonacic-Koutecky, P.Fantucci and J. Koutecky, J. Chem. Phys. 93, 3802 (1990)

FIGURE CAPTIONS

Figure1. Mass distribution of silver clusters Ag_N^+ up to cluster size N = 100 plotted in logarithmic scale. Two kinds of anomalies are observed superimposed on the pseudo-exponential decrease of the ion intensity. One is the odd-even alternation and the other is a steep decrease in the ion intensity at the magic numbers N = 3, 9, 21, 35, 41, 59 and 93.

Figure 2. Secondary ion mass spectrum of silver clusters (Ag_N^+) from N = 50-250.

Figure 3. Size distribution of copper clusters: Cu_N^- (upper curve) and Cu_N^+ (lower curve), plotted on a logarithmic scale.

Figure 4. Visualization of the ionization of an initially neutral (left side) and initially negatively charged particle.

Figure 5. Simplified scheme of the photoejection process within the frozen orbital picture: Laser at fixed energy ionizes an electron from the HOMO (highest occupied molecular orbital) (1) or from a deeper orbital (2). The electron energies, E_{kin}, are a direct measure of the orbital positions. In ground-state (cluster) anions the additional electron occupies the LUMO (Lowest unoccupied molecular orbital) if the corresponding neutral cluster has a closed-shell configuration. In this case a photoelectron of higher kinetic energy will be emitted

Figure 6. Photoelectron spectra of Ag_N^-, N = 3-20, at a detachment energy of 3.68 eV. The arrows indicate the positions of first strong maxima

Figure 7. Measured Ag_N^- photodetachment energies[4]

Figure 8. Calculated Cu_N electron affinities within the spheroidal jellium model[5], compared to measured photodetachment thresholds

Figure 9. UPS of negative copper clusters in the 1-410 atom size range, taken with an F_2 excimer laser at 7.9 eV.

Figure 10. Electron affinities and 3d band energy onsets of copper clusters as a function of 1/R (R = cluster radius). The black solid bars on the left hand side refer to the range of measured work functions and corresponding 3d band onsets.

Figure 11. Electronic structure of icosahedral Cu_{13} (b) and Cu_{12}(e) clusters. The Mulliken charge analysis (d character of the levels) is given in (a) for Cu_{13}. (c) and (d) gives the electronic levels of Cu_{13} and Cu_{12} using a simple spherical potential with appropriate parameters and one single electron per atom

Figure 12. Contour map of the charge distribution of 3d orbitals (a) and 4s, 4p orbitals (b) in Cu_{13}.

Figure 13. Energy levels of octahedral clusters. The d-character of levels is shown by light lines. The left and right edges of levels show 0% and 100% d-character respectively. (a) Cu_6 octahedron, (b) Cu_8 cube, (c) C_{13} cuboctahedron, (d) C_{15} rhombic dodecahedron, (e) Cu_{19} combined cluster of cuboctahedron and octahedron.

Figure 14. Universal plot comparing metal cluster ionization potential data sets with the predictions of eq. (7). R is estimated from bulk atomic volumes and W is an extrapolation of the data to 1/R=0

Figure 15. Differences between experimental photodetachment energies (as estimates of upper bounds of electron affinities) and bulk work function versus the reciprocal of the cluster radius R for Al_N, In_N and Tl_N. The straight line gives the expected behavior according to eq.(8).

Figure 16. Experimental electron affinities as a function of cluster size. The smooth lines represent the prediction of the spherical drop model for Cu_N (solid) and Ag_N (dashed). (Ref. 24).

Figure 17. Photoionization efficiency curves at 20 mm resolution for Na_N (14<N<21). There is a systematic even-odd effect in post-threshold ion signal (near 240 mm). These fluctuations are due to variations in fragmentation rate. The implication is that even cluster ions are slightly less stable than their odd neighbors.

Figure 18. Comparison of Hückel (full circles), Density functional-Local Spin Density (open circles) and experimental (solid line) ionization potentials for Na and K clusters. Also shown is expression (7).

Figure 19. The binding energy per atom of Na_N^+ clusters calculated by CI methods. The important Molecular Orbital energy levels are schematically shown and the electronic occupation is indicated.

Figure 20. Evolution of the Molecular Orbital energy levels with cluster size. The notation s,p,d,f, etc reflects the nodal character of the orbitals. The calculations were performed by the Hückel method and the data correspond to the most stable geometry calculated for each cluster size. PL and S denote planar and spherical structures; OE and PE pertain to oblate and prolate ellipsoids respectively. All energies are in Hückel units (hu) (ref. 25).

TABLE I

Shell-closing effect observed in the mass spectra of the positive and negative clusters of copper, silver, and gold. The shell closing effect is observed at the $(N_S + 1)$ mer in the case of positive clusters and at the $(N_S - 1)$ mer for negative clusters, where N_S is the shell closing number.

N_S	Configurations	Copper		Silver		Gold	
		$(Cu)_N^+$	$(Cu)_N^-$	$(Ag)_N^+$	$(Ag)_N^-$	$(Au)_N^+$	$(Au)_N^-$
2	$1s$	○		○	○	○	×
8	$1p$	○	○	○	○	○	×
18	$1d$	△	△	△	△	△	○
20	$2s$	○	○	×	○	○	×
34	$1f$	○	○	○	○	○	○
40	$2p$	○	○	○	○	×	×
58	$1g$	○	○	○	○	○	○
92	$2d, 1h, 3s$	○	○	○	×	○	○
138	$2f, 1i, 3p$	○	△	○	○	○	△
198	$2g, 1j, 3d, 4s$			○	△		

○ = observed clear shell closing effect
△ = observed weak shell closing effect
× = not observed

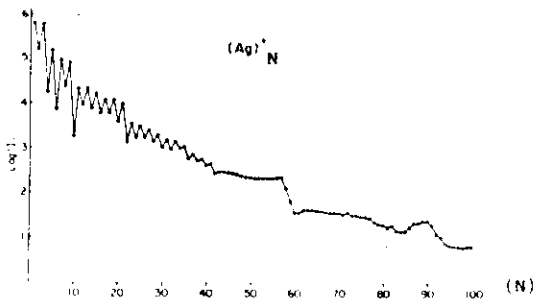

Fig. 1. Mass distribution of silver clusters $(Ag)_N^+$ up to cluster size $N = 100$ plotted in logarithmic scale. Two kinds of anomalies are observed superimposed on the pseudo-exponential general decrease of the ion intensity. One is odd–even alternation and the other is a steep decrease in the ion intensity at the "magic" numbers 3, 9, 21, 35, 41, 59 and 93.

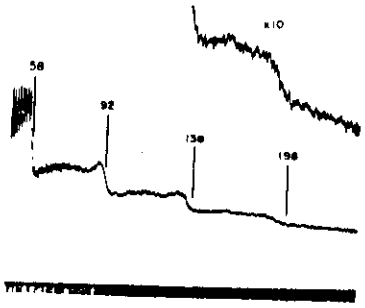

Fig. 2. Secondary-ion mass spectrum of silver clusters $(Ag)_N^+$ from $N = 50$–250 recorded by a UV recorder. The resolved peaks to each cluster are obtained until $N = 100$.

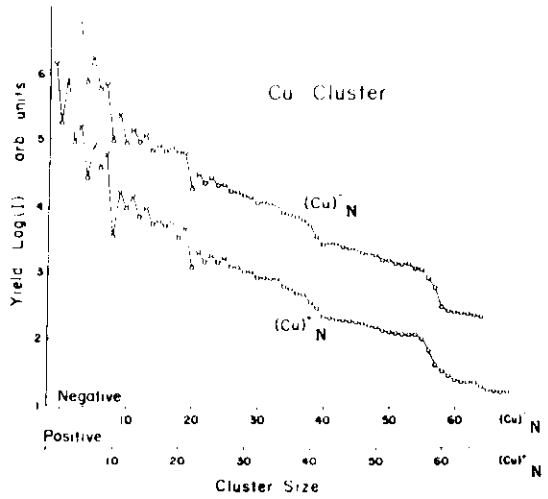

Fig 3 Size distributions of copper clusters, $(Cu)^-_N$ (upper curve) and $(Cu)^+_N$ (lower curve), plotted on a logarithmic scale

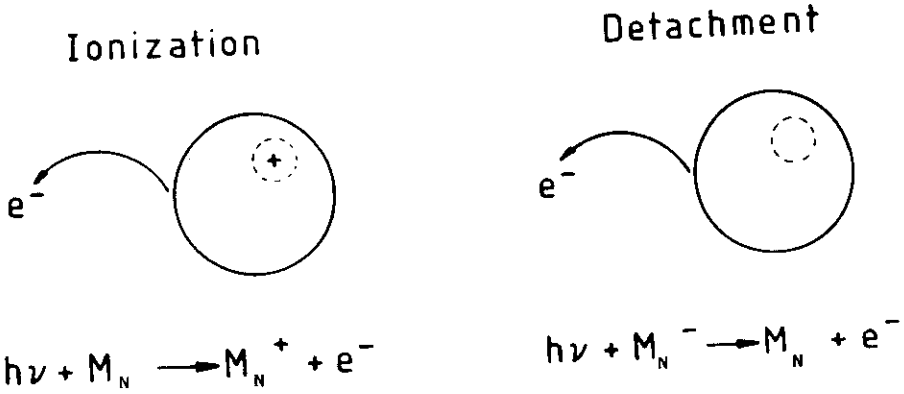

Fig. 4

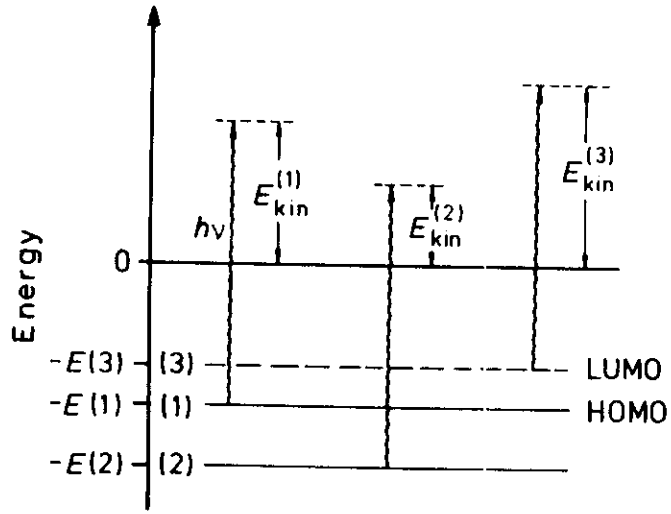

Fig. 5

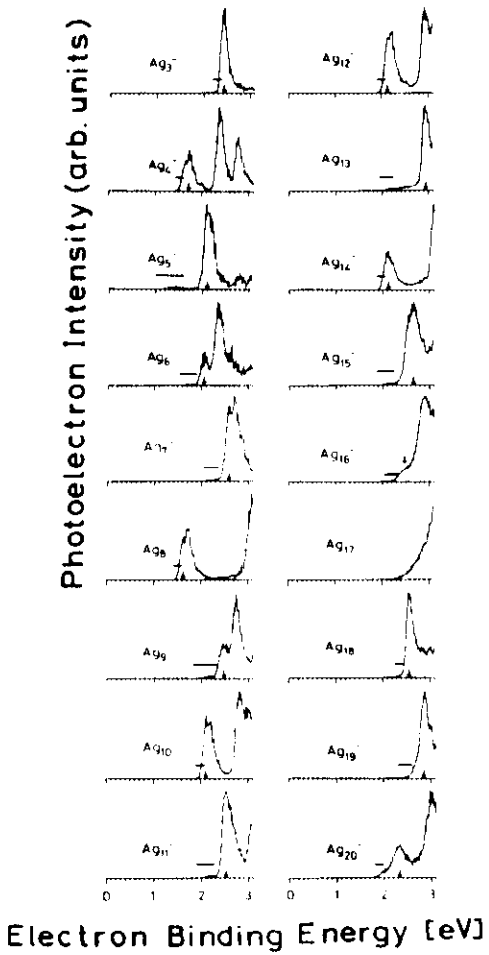
Photoelectron Intensity (arb. units)
Ag3-
Ag4-
Ag5-
Ag6-
Ag7-
Ag8-
Ag9-
Ag10-
Ag11-
Ag12-
Ag13-
Ag14-
Ag15-
Ag16-
Ag17-
Ag18-
Ag19-
Ag20-
0 1 2 3
0 1 2 3
Electron Binding Energy [eV]

Fig 6

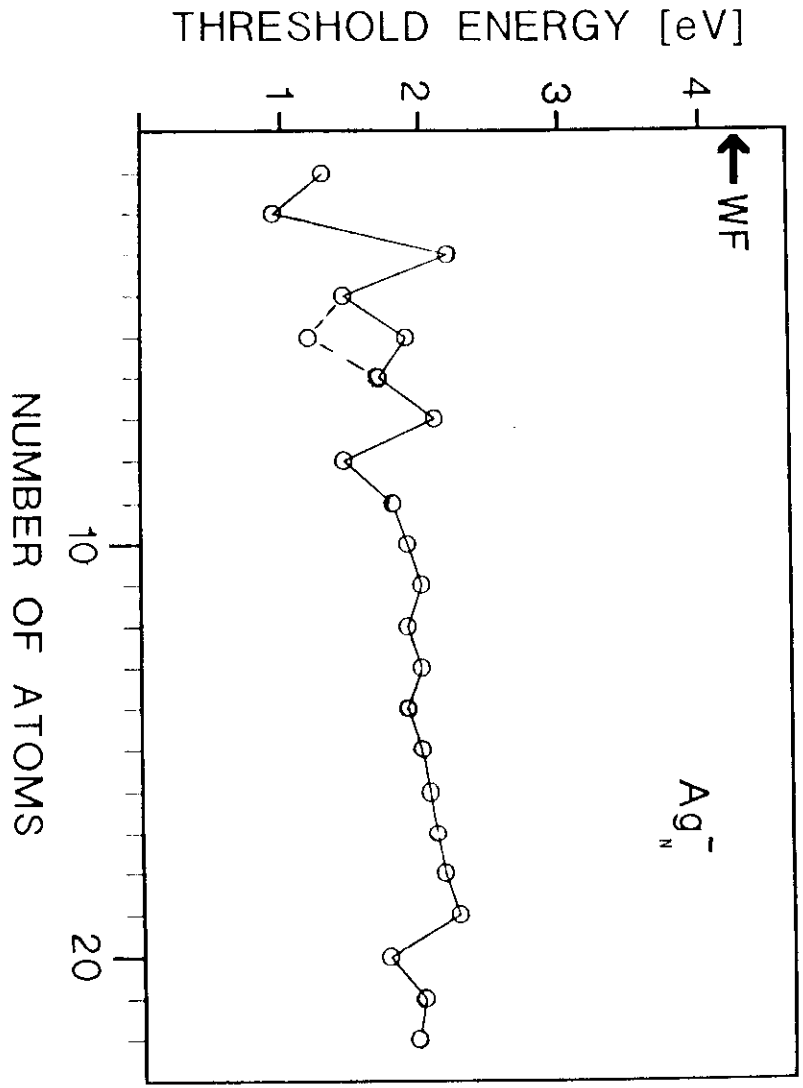
THRESHOLD ENERGY [eV]
1
2
3
4
WF
NUMBER OF ATOMS
10
20
Ag-N

Fig 7

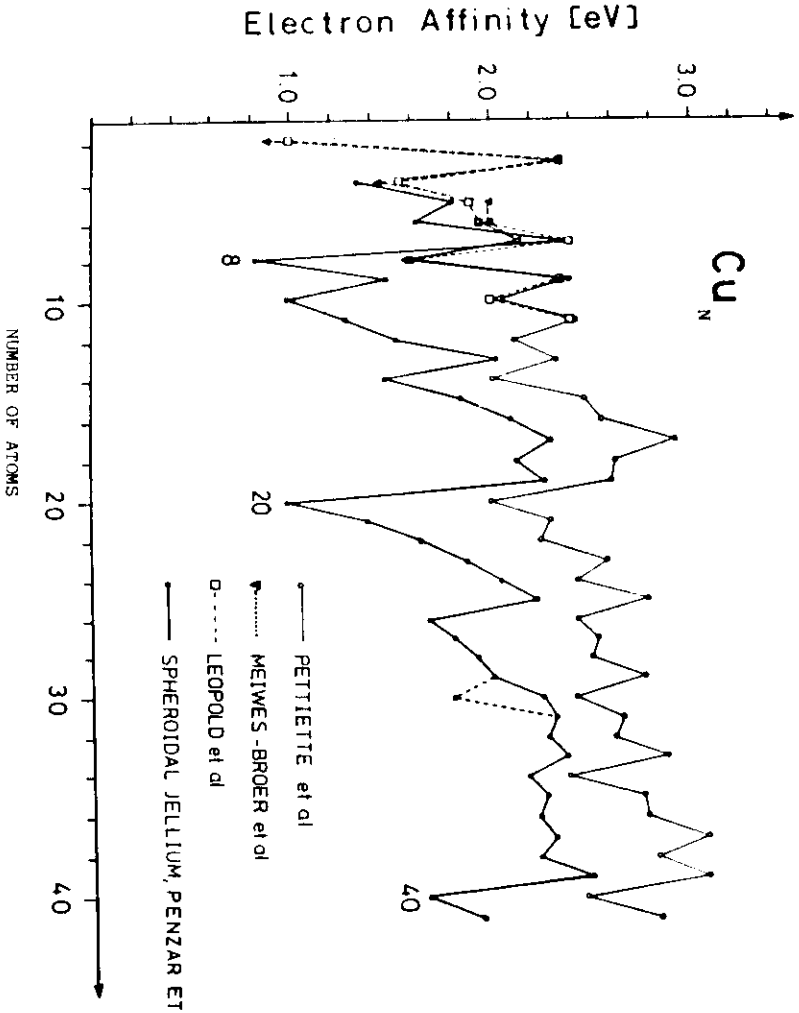
Electron Affinity [eV]
1.0
2.0
3.0
8
10
20
30
40
Cu_N
NUMBER OF ATOMS
PETTIETTE et al
MEIWES-BROER et al
LEOPOLD et al
SPHEROIDAL JELLIUM, PENZAR ET AL.

Fig. 8

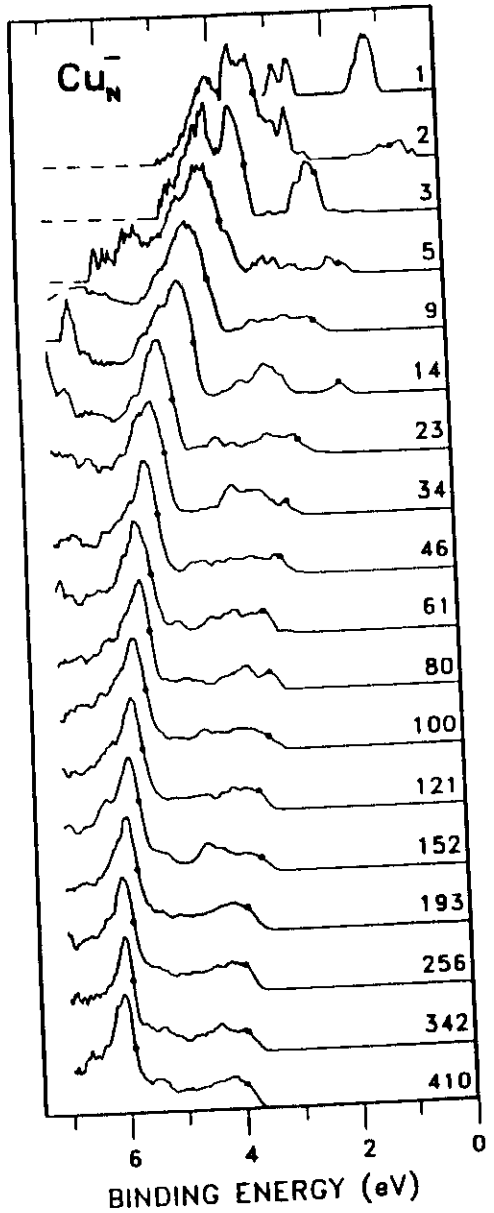
Cu_N^-
1
2
3
5
9
14
23
34
46
61
80
100
121
152
193
256
342
410
6
4
2
0
BINDING ENERGY (eV)

Fig. 9

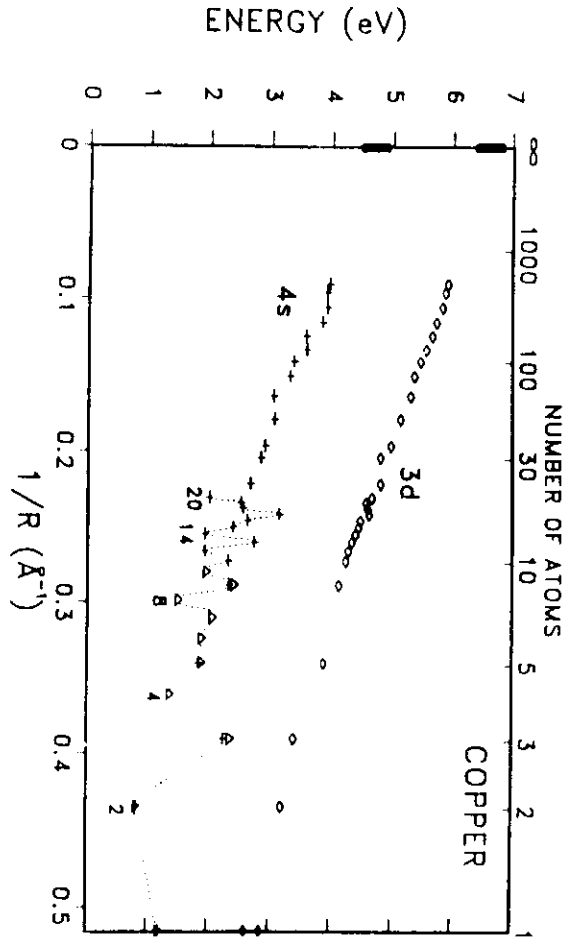

Fig 10

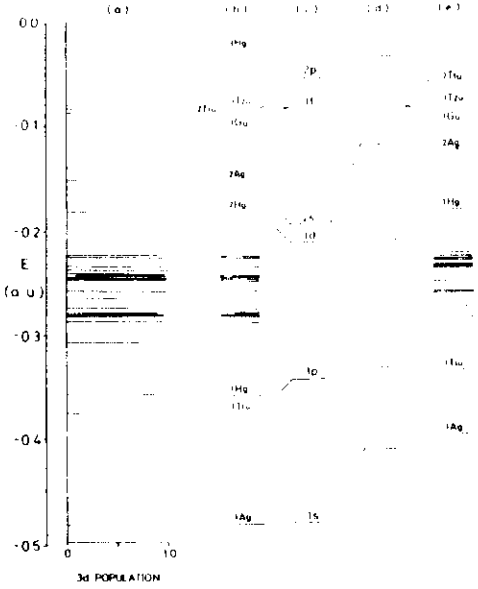

Fig 11

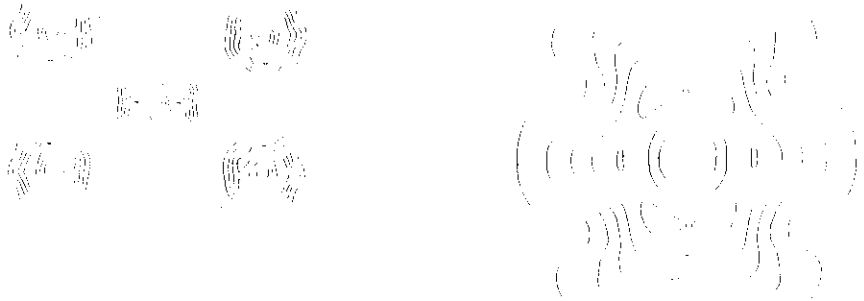

(a) (b)

Fig 12

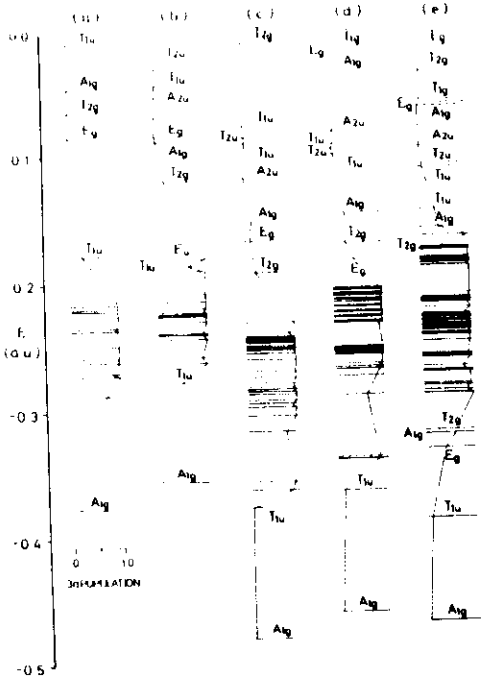

Fig. 13. Energy levels of octahedral clusters. The *d*-character of levels is shown by light lines. The left and right edges of levels show 0% and 100% *d* character, respectively. (a) Cu_6 octahedron, (b) Cu_8 cube, (c) Cu_{13} cuboctahedron, (d) Cu_{15} rhombic dodecahedron, and (e) Cu_{19} combined cluster of cuboctahedron and octahedron.

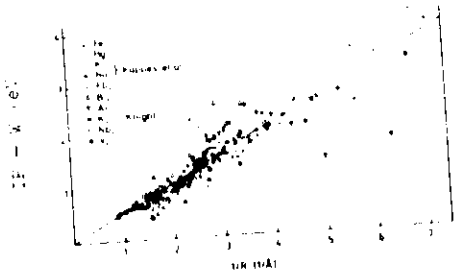

Fig 14

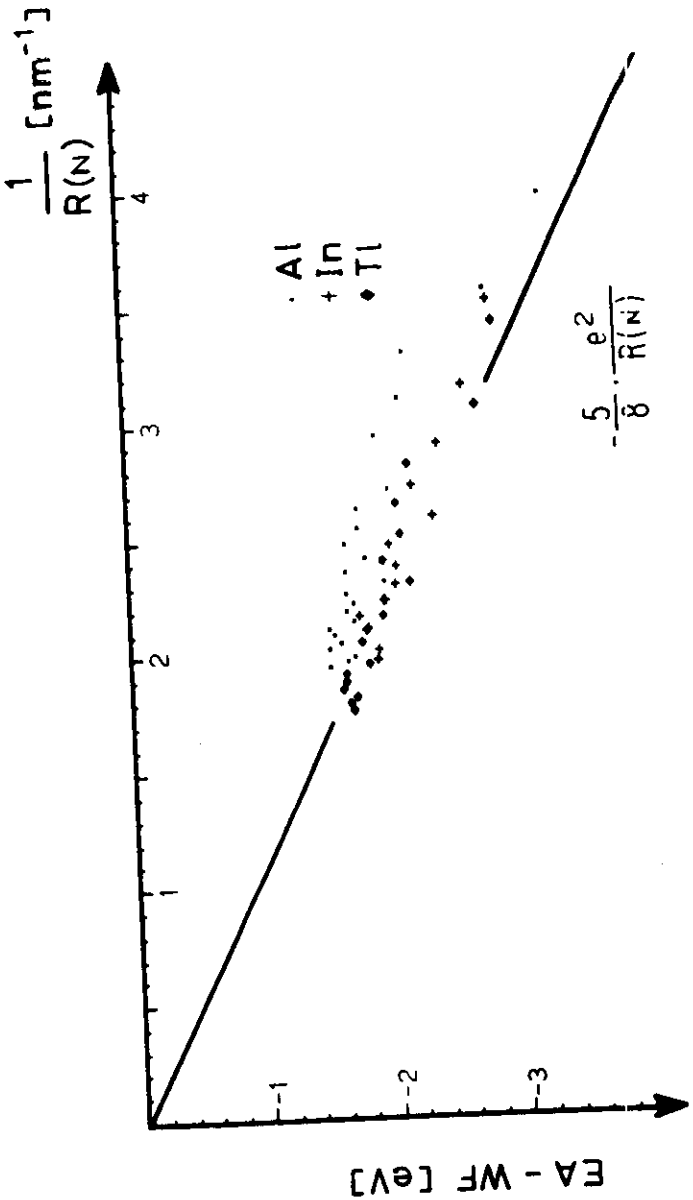

Fig 15

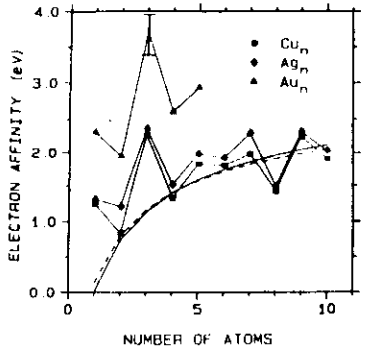

Fig 16

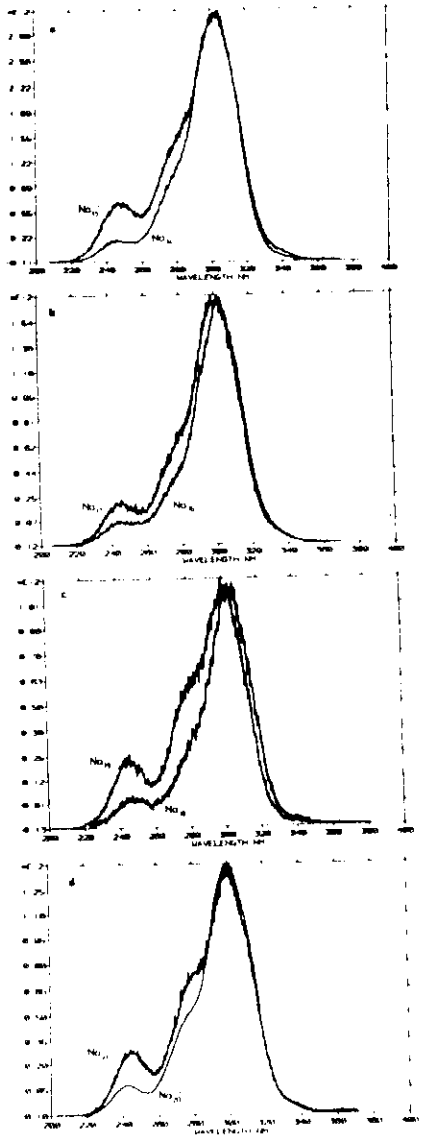

Fig 17

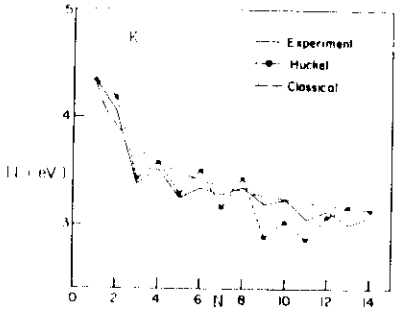

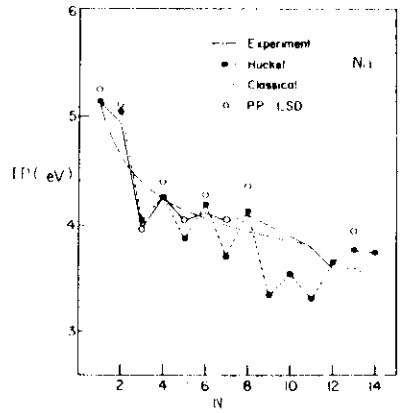

Fig 18

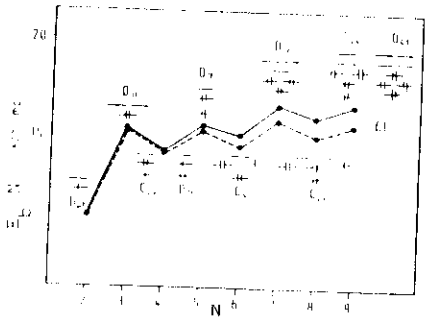

Fig 19

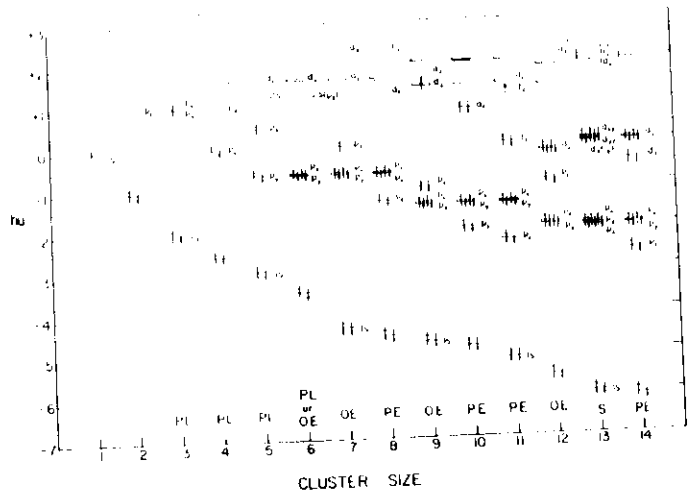
PL
PL
PL
PL or OE
OE
PE
OE
PE
PE
OE
S
PE
1
2
3
4
5
6
7
8
9
10
11
12
13
14
CLUSTER SIZE

Fig. 20